

Superfluid to Mott-insulator transition of hardcore bosons in a superlattice

Itay Hen* and Marcos Rigol†

Department of Physics, Georgetown University, Washington, DC 20057, USA

(Dated: November 12, 2018)

We study the superfluid to Mott-insulator (SF-MI) transition of hardcore bosons in commensurate superlattices in two and three dimensions. We focus on the special case where the superlattice has period two and the system is at half filling. We obtain exact numerical results by using the stochastic series expansion (SSE) algorithm, and compute various properties of the system, such as the ground-state energy, the fraction of bosons in the zero-momentum mode, the superfluid density, and the compressibility. With finite-size scaling, we find the critical points of the phase transition. We also explore the extent to which several approximate solutions such as mean-field theory, with and without spin-wave corrections, can help one gain analytical insight into the behavior of the system in the vicinity of the phase transition.

PACS numbers: 64.70.Tg, 03.75.Lm, 02.70.Ss, 67.85.-d

Keywords: superfluidity, Mott-insulator, hardcore bosons

I. INTRODUCTION

Recent developments in the field of ultracold Bose gases have opened a new promising avenue of theoretical and experimental research in the study of the phases of quantum matter. A gas of bosonic atoms in an optical trap has been reversibly tuned from a Bose-Einstein condensate to a state composed of localized atoms as the strength of a periodic optical potential was varied.^{1,2} This is an example of a quantum phase transition; a phase transition generated by quantum fluctuations and correlations rather than by a competition between the energy of a system and the entropy of its thermal fluctuations.³ Understanding this phenomenon has emerged as one of the most challenging and interesting tasks of condensed matter physics. Theoretically, it is generally accepted that it can be studied using the Bose Hubbard model, where the transition is thought to be from a superfluid phase to a Mott-insulator (SF-MI), as examined in the seminal paper by Fisher *et al.*,⁴ with an application to ⁴He absorbed in porous media in mind. The relevance of the Bose-Hubbard model to gases of alkali-metal atoms in optical lattices was realized in Ref. 5, and recent developments have been reviewed in Refs. 6,7.

Interestingly, the Bose-Hubbard model is nonintegrable even in one dimension (as opposed to, say, its fermionic counterpart⁸). Gaining analytical insight into the SF-MI phase transition thus normally requires resorting to numerical and variational methods for a better understanding of this phenomenon. Within the latter approach, the phase transition is taken to be the point at which the variational ansatz has lower energy than a delocalized Bogoliubov state (where a fixed particle number at each lattice site is constrained).

In a recent paper, Aizenman *et al.*⁹ considered an alternative model for the study of the SF-MI phase transition. They studied the half-filled Bose-Hubbard model in the limit of infinite on-site repulsion (i.e., the case of hardcore bosons), in the presence of an alternating on-site chemical potential (a superlattice with period two). They

showed that this model exhibits all the salient properties apparent in the Bose-Hubbard model, while also being more ‘treatable’ analytically. Specifically, they were able to rigorously prove the existence of superfluid and Mott-insulating phases in three dimensions. In addition, it is also known that this very same model is exactly solvable in one-dimension through a mapping to noninteracting fermions. In this case, the half-filled system is insulating for any nonzero alternating potential.¹⁰ The off-diagonal one-particle correlations and the momentum distribution function of this model, as well as its nonequilibrium dynamics, were computed by exact means¹¹ in Ref. 12.

Motivated by the aforementioned results, here we study the SF-MI phase transition of hardcore bosons in the presence of an alternating potential in two and three dimensions. We focus on the case where the system is at half-filling, in which case the transition between the superfluid state and the insulating state occurs at fixed density. Our first goal is to accurately determine the critical values of the alternating potential strength at which the phase transition takes place. As a next step, we analyze the results of different approximate solutions, such as mean-field theory with and without the addition of spin-wave corrections, as these allow for an analytical treatment of the problem.

Our approach is to first perform high-precision numerical simulations using the stochastic series expansion (SSE) algorithm^{13,14} in order to find the critical points of the superfluid to Mott-insulator phase transition in the various dimensions. The quantities we calculate are the free energy Ω , the fraction of bosons in the zero-momentum mode ρ_0 ,²⁹ the superfluid density ρ_s and the compressibility $\kappa = \partial\rho/\partial\mu$. The latter three quantities signify the transition from a superfluid to an insulator by dropping to zero at this point (while having nonzero values in the superfluid regime). We then employ mean-field and spin-wave analyses, which allow for some analytical insight into the behavior of our observables of interest and the location of the critical point. Our using these approximation methods is partly motivated by results

previously reported by Bernardet *et al.*,¹⁵ who studied the homogeneous version of the model in two dimensions. There, the mean-field approximation alone was shown to provide a fairly good qualitative description of the model, and remarkably enough, when spin-wave corrections were added, quantities such as the superfluid density and the condensate fraction were found to be virtually indistinguishable from their exact-numerical counterparts.

The paper is organized as follows. In Sec. II we briefly review the model at hand. In Sec. III, we present the exact numerical solutions obtained using the stochastic series expansion (SSE) algorithm. We compute the various physical quantities at zero temperature, and find the critical values of the SF-MI phase transition. In Sec. IV we proceed to study several approximation schemes, namely mean-field approaches and spin-wave corrections, comparing the critical values obtained using these methods, with the exact results. In Sec. V we conclude with a few comments and several remarks regarding future work.

II. THE MODEL

The Hamiltonian for hardcore bosons in a period-two superlattice in d -dimensions, with $N = L^d$ sites and periodic boundary conditions, can be written as:

$$\hat{H} = -t \sum_{\langle ij \rangle} (\hat{a}_i^\dagger \hat{a}_j + \hat{a}_j^\dagger \hat{a}_i) - A \sum_i (-1)^{\sigma(i)} \hat{n}_i - \mu \sum_i \hat{n}_i. \quad (1)$$

Here, $\langle ij \rangle$ denotes nearest neighbors, \hat{a}_i (\hat{a}_i^\dagger) destroys (creates) a hardcore boson on site i , $\hat{n}_i = \hat{a}_i^\dagger \hat{a}_i$ is the local density operator, μ is the global chemical potential, and $A(-1)^{\sigma(i)}$ is an alternating local potential with $\sigma(i) = 1$ on the odd sublattice and -1 on the even sublattice. The hopping parameter t sets the energy scale.

The hardcore boson creation and annihilation operators satisfy the constraints

$$\hat{a}_i^{\dagger 2} = \hat{a}_i^2 = 0, \quad \{\hat{a}_i, \hat{a}_i^\dagger\} = 1, \quad (2)$$

which prohibit double or higher occupancy of lattice sites, as dictated by the $U \rightarrow \infty$ limit of the Bose-Hubbard model. For any two different sites $i \neq j$, the creation and annihilation operators obey the usual bosonic relations

$$[\hat{a}_i, \hat{a}_j] = [\hat{a}_i^\dagger, \hat{a}_j^\dagger] = [\hat{a}_i, \hat{a}_j^\dagger] = 0. \quad (3)$$

The expected phase diagram of the model, in dimensions higher than one, is sketched in Fig. 1. Our model has two (trivial) Mott-insulating regimes corresponding to a completely filled lattice (with particle density $\rho = 1$), obtained for large and positive chemical potential values, and a second insulating regime which corresponds to an

empty lattice, formed in the case where the chemical potential is large and negative. These two regimes are also present in the absence of the alternating potential. The alternating one-body potential creates another insulating phase, one for which the density of particles is $\rho = 1/2$. In this case, the alternating potential, will in some cases (depending on its strength) create a gap in the energy spectrum, generating a superfluid to Mott-insulator transition. As the latter regime is the one which is of interest to us, we shall henceforth set the global chemical potential to $\mu = 0$. In this case, the model has particle-hole symmetry which in turn fixes the density at $\rho = 1/2$ as desired.

Before moving on, a remark is in order. The $\rho = 1/2$ insulating phase of the model at hand is a consequence of a counterbalance between strong on-site interactions (which in our model are in fact infinite) and an alternating potential. The resulting local density will thus be different on the odd sublattice than on the even sublattice. While this state is sometimes referred to as a charge density wave,¹⁰ in what follows, we shall address this phase as a Mott-insulator, in the spirit of Ref. 9.

III. EXACT NUMERICAL RESULTS

We obtain numerically-exact results for the model at hand by performing numerical simulations based on the stochastic series expansion (SSE) algorithm.^{13,14} As our main objective is to find the critical points of the SF-MI phase transition in the various dimensions, simulations

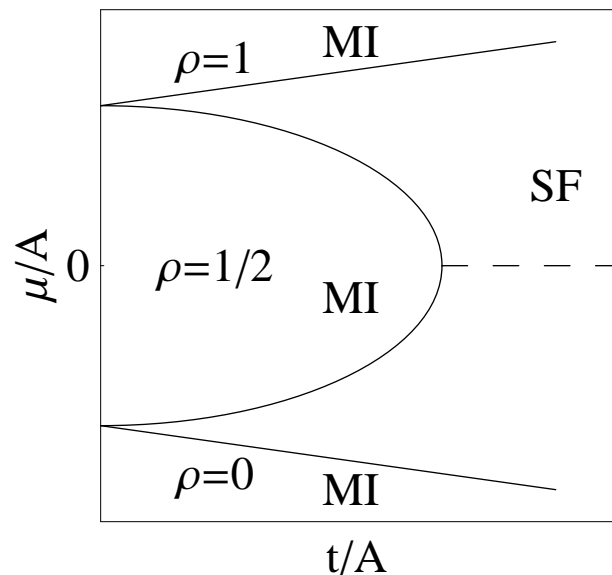


FIG. 1: Qualitative description of the expected phase diagram of the model at hand, Eq. (1). The diagram contains three Mott-insulating (MI) regions corresponding to zero, half and full filling, and a superfluid (SF) phase.

are performed for a range of values of the ratio A/t and for various system sizes. Since we are interested in the zero-temperature properties of the system, simulations are performed with high inverse-temperature $\beta = 1/T$ (in our units, $k_B = 1$), where in most cases we will find it sufficient to have $\beta \geq 2L$ in order to obtain virtually zero-temperature results. (The effects of increasing β beyond this value are indiscernible.)

Finite size effects are corrected by repeating the simulations with different system sizes. The thermodynamic-limit value of the phase transition is then extrapolated by performing finite size scaling of the results in the vicinity of the phase transition: Around the critical point, most physical quantities (which we denote here by X) scale according to the general rule:

$$XL^{\xi/\nu} = F(|A - A_c|L^{1/\nu}), \quad (4)$$

where F is a universal scaling function, $A - A_c$ is the shifted control parameter (A being the control parameter, and A_c – the critical value), ν is the correlation length critical exponent and ξ is the critical exponent belonging to the observable X . The values of these exponents are determined by the universality class the transition belongs to. In our case (and in the Bose-Hubbard model as well), it is the $(d + 1)$ dimensional XY universality class.^{4,16} Eq. (4) will help us find the critical point, as it tells us that (a) the quantity $XL^{\xi/\nu}$ should be independent of the system-size at the phase transition, and (b) when plotting $XL^{\xi/\nu}$ against $|A - A_c|L^{1/\nu}$ the resulting curve should be independent of the system-size as well.

The quantity we shall be using to that end is the superfluid density, which has the critical exponent $\xi = \nu(d + z - 2)$ (see Ref. 4 for details) where d is the dimension, and z is the dynamical critical exponent, which in our case is $z = 1$.¹⁶ The correlation length exponent ν is dimension-dependent and takes the values 1, 0.672 and 0.5 in one, two and three dimensions, respectively.

A. One dimension

In one dimension, our model has an analytic solution.¹⁰ This is due to the Jordan-Wigner transformation which enables the mapping of the hardcore bosons Hamiltonian to that of noninteracting spinless fermions.¹⁰ The latter Hamiltonian may be diagonalized to produce exact analytical results. In this case, the SF-MI phase transition occurs at $A_c/(2dt) = 0$. We performed simulations in one dimension as well, as a check on our computational method. No discrepancy between the analytical solution and the numerical one were found: In Fig. 2, the superfluid density is plotted against $A/(2dt)$ for different system sizes (here, $\beta = 500$). In the figure, all curves intersect at the critical point $A_c/(2dt) = 0$, indicating the location of the phase transition in the thermodynamic limit, in agreement with the analytic results. The inset shows the scaled superfluid density as a function of the scaled control parameter, in which case all curves

should be, and in fact are, on top of each other. The numerical value for the superfluid density at the transition coincides with the expected value of π^{-1} given by the analytic solution.¹⁰

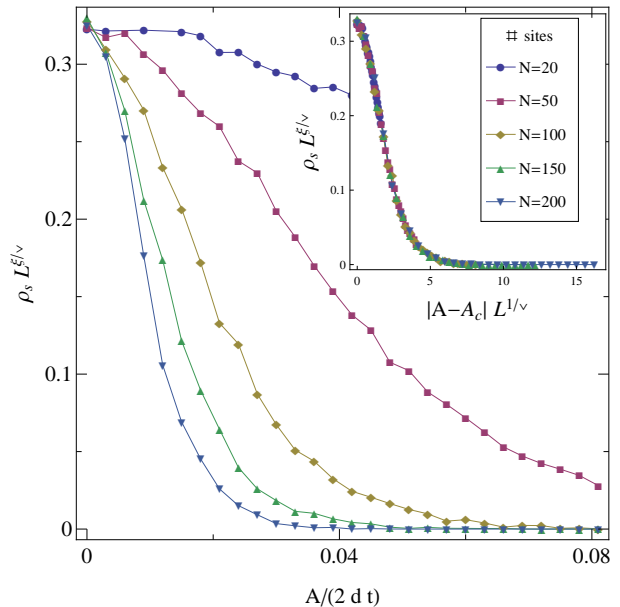


FIG. 2: (Color online) Scaled superfluid density as a function of $A/(2dt)$ for the various system sizes in the one-dimensional case. The intersection at $A/(2dt) = 0$ indicates the location of the SF-MI phase transition. In the inset, the control parameter (the horizontal axis) is scaled as well, leading to the collapse of all data points into a single curve.

As superlattices such as the one we study here have already been realized in experiments with ultracold bosons in optical lattices,^{17,18,19,20} and the observable usually measured in those kind of experiments is the momentum distribution function $n(k)$, we plot it in Fig. 3 for two different values of A/t . Due to the quasi-long-range decay of one-particle correlations in the superfluid phase, the momentum distribution function has a peak at $k = 0$ [Fig. 3(a)]. On the other hand, in the insulating phase, the one-particle correlations decay exponentially, yielding a broad momentum distribution [Fig. 3(b)]. This leads to the following observation: As one increases the size of the lattice, one finds that in the superfluid phase $n(k)$ increases for small values of k [Fig. 3(a)], while for the insulating phase [Fig. 3(b)] this does not happen. Exact results for $n(k)$ (using the approach described in Ref. 11), are also presented in Fig. 3. As expected, the SSE results are right on top of the exact ones.

B. Two dimensions

In dimensions higher than one, no analytic solution to the model exists, so exact results are obtainable only numerically. Here, we have applied the SSE algorithm to

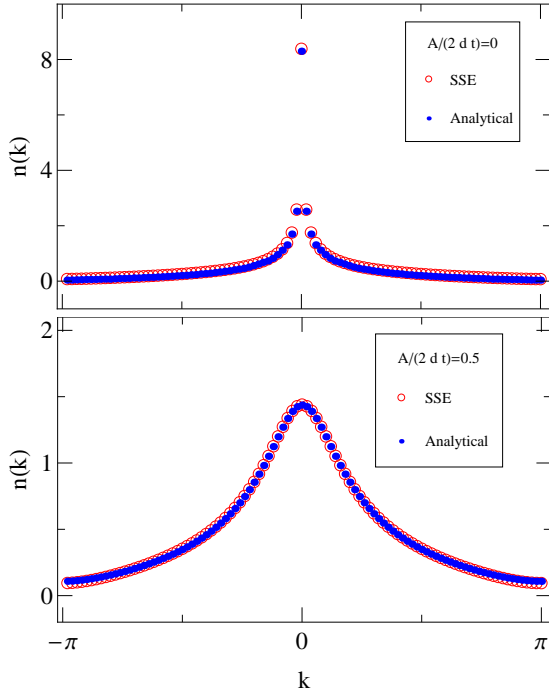


FIG. 3: (Color online) Momentum distribution function $n(k)$ in the superfluid regime (top) and in the insulating regime (bottom) for the one-dimensional system with 100 sites. In both cases, the SSE results (empty circles) are on top of the analytical ones (full circles), serving as an indication to the accuracy of our computational method.

systems of sizes ranging from 10×10 to 64×64 , with inverse-temperature $\beta = 96$. In Fig. 4, the scaled superfluid density is plotted against $A/(2dt)$ for the different system sizes (the errors are of the order of magnitude of the symbol sizes). All curves intersect at $A_c/(2dt) = 0.495(\pm 0.004)$, signifying the phase transition. The inset shows the scaled superfluid density as a function of the scaled control parameter. As in the one-dimensional case, all data points fall into a single curve. The value for the critical point we obtained here agrees with the value recently obtained by Priyadarshie *et al.*²¹

The momentum distribution function in the superfluid and insulating regimes are shown in Figs. 5(a) and 5(b), respectively. In two dimensions, the superfluid regime exhibits true off-diagonal long-range order, which means that the $n(k=0)$ peak is sharper than in one dimension. This can be seen in Fig. 5(a). The Mott-insulating regime is once again characterized by an exponential decay of one-particle correlations. The corresponding momentum distribution function has a broad peak around $n(k=0)$ as shown in Fig. 5(b).

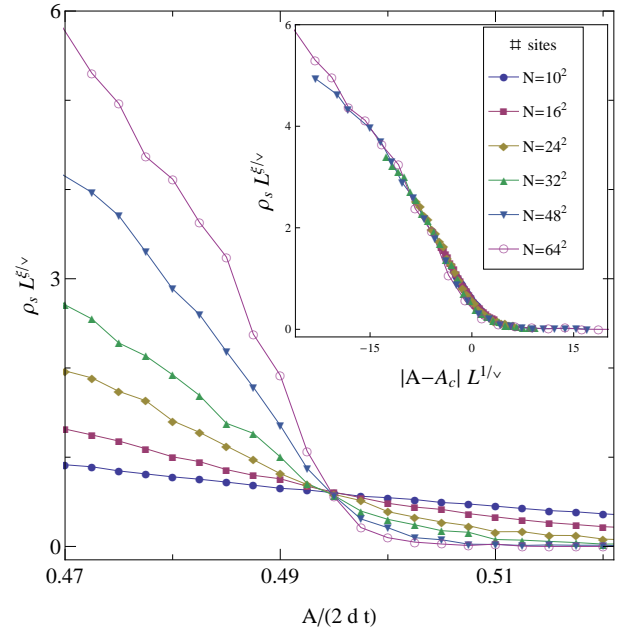


FIG. 4: (Color online) Scaled superfluid density as a function of $A/(2dt)$ for the various system sizes in the two-dimensional case. The intersection at $A_c/(2dt) \approx 0.495$ indicates the occurrence of the phase transition at that point. In the inset, the control parameter (the horizontal axis) is scaled as well, leading to the collapse of all data points into a single curve.

C. Three dimensions

In three dimensions, we have performed simulations for system sizes ranging from $6 \times 6 \times 6$ to $20 \times 20 \times 20$ and an inverse temperature of $\beta = 40$. Here, the SF-MI phase transition is found at $A_c/(2dt) = 0.693(\pm 0.005)$, as indicated by the scaled superfluid density plotted as a function of $A/(2dt)$ in Fig. 6, for the different system sizes. The inset in Fig. 6 depicts the scaled superfluid density as a function of the scaled control parameter, exhibiting the collapse of all data points into a single curve, as in one and two dimensions. The momentum distribution function in three dimensions is qualitatively similar to its two-dimensional counterpart, both in the superfluid phase and in the insulating phase, and thus will not be presented here.

IV. APPROXIMATION SCHEMES

Having obtained the exact critical values via quantum Monte Carlo techniques, we now turn to look for approximation schemes that would provide analytical descriptions of the phase transition. We start this investigation with the Gutzwiller mean-field approach. Before doing so however, we recall that the model at hand can also be viewed as the XY model of a spin-1/2 system.²² We shall make use of this correspondence, utilizing the exact

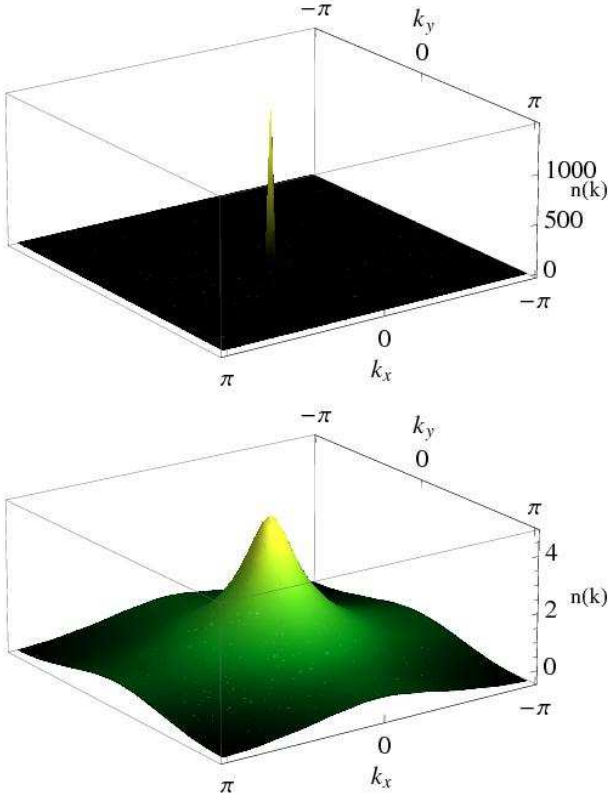


FIG. 5: (Color online) Momentum distribution function $n(k)$ in the superfluid regime $A/(2dt) = 0.1$ (top) and in the insulating regime $A/(2dt) = 0.7$ (bottom) for a 64×64 system and $\beta = 96$.

mapping between bosonic operators and $SU(2)$ generators, namely,

$$\begin{aligned} \hat{a}_i^\dagger &\leftrightarrow S_i^+, \\ \hat{a}_i &\leftrightarrow S_i^-, \\ \hat{a}_i^\dagger \hat{a}_i &\leftrightarrow S_i^z + 1/2. \end{aligned} \quad (5)$$

With this mapping, the hardcore bosons Hamiltonian, Eq. (1), becomes that of the XY antiferromagnet with an alternating magnetic field applied along the \hat{z} direction:

$$\begin{aligned} \hat{H} = & -t \sum_{\langle ij \rangle} (S_i^+ S_j^- + S_j^+ S_i^-) \\ & - \sum_i \left(\mu + A(-1)^{\sigma(i)} \right) \left(S_i^z + \frac{1}{2} \right). \end{aligned} \quad (6)$$

A. Mean-field approach

We start our mean-field calculation with the following product state as an initial ansatz:

$$|0\rangle_{\text{MF}} = \bigotimes_j \left(\sin \frac{\theta_j}{2} |\downarrow\rangle + \cos \frac{\theta_j}{2} e^{i\varphi_j} |\uparrow\rangle \right), \quad (7)$$

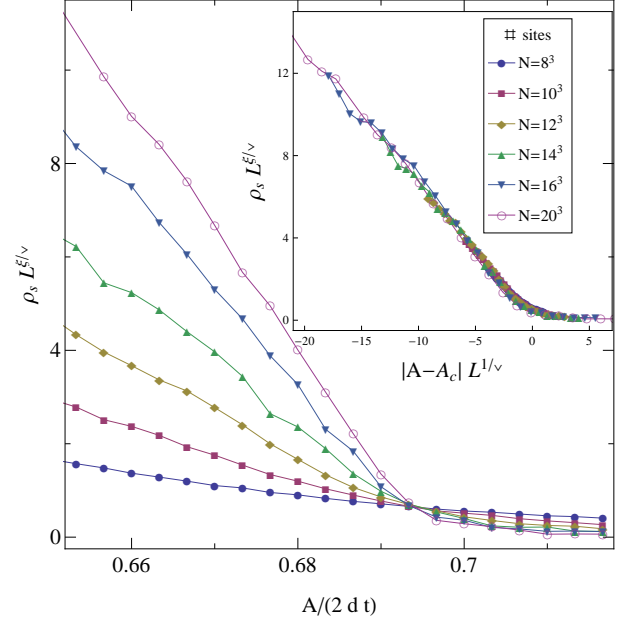


FIG. 6: (Color online) Scaled superfluid density as a function of $A/(2dt)$ for the various system sizes in the three-dimensional case. The intersection at $A_c/(2dt) \approx 0.693$ indicates the location of the SF-MI phase transition. In the inset, the control parameter (the horizontal axis) is scaled as well, leading to the collapse of all data points into a single curve.

where (θ_j, φ_j) specify the orientation of the j -th spin. Obviously, we expect every other site to be described by the same wave function, due to the symmetry of the problem. This is schematically shown in Fig. 7. As we

$ \psi_2\rangle$	$ \psi_1\rangle$	$ \psi_2\rangle$	$ \psi_1\rangle$
$ \psi_1\rangle$	$ \psi_2\rangle$	$ \psi_1\rangle$	$ \psi_2\rangle$
$ \psi_2\rangle$	$ \psi_1\rangle$	$ \psi_2\rangle$	$ \psi_1\rangle$
$ \psi_1\rangle$	$ \psi_2\rangle$	$ \psi_1\rangle$	$ \psi_2\rangle$

FIG. 7: A schematic description of the product state in the mean-field approach in two dimensions. Every other site is described by the same wave function.

are using the grand-canonical scheme, the orientations of the spins will be determined by minimizing the grand-

canonical potential (per site)

$$\Omega_{\text{MF}} = {}_{\text{MF}}\langle 0 | \hat{H} | 0 \rangle_{\text{MF}} = -\frac{t}{2N} \sum_{\langle ij \rangle} \sin \theta_i \sin \theta_j \cos(\phi_i - \phi_j) - \frac{1}{2N} \sum_i \left(\mu + A(-1)^{\sigma(i)} \right) (1 + \cos \theta_i). \quad (8)$$

with respect to these angles. For the azimuthal angles, this simply implies a constant (yet arbitrary) value $\varphi_j = \Phi$, while for the polar angles, extremization yields

$$\cos \theta_1 = \mu_1 \sqrt{\frac{1 + \mu_2^2}{1 + \mu_1^2}}, \quad (9a)$$

$$\cos \theta_2 = \mu_2 \sqrt{\frac{1 + \mu_1^2}{1 + \mu_2^2}}, \quad (9b)$$

where $\mu_{1,2} \equiv (\mu \pm A)/(2dt)$. These values correspond to a minimal configuration only in the region $|\mu_1 \mu_2| < 1$. Outside this region, the system is saturated, and the solution is one where all spins are aligned – pointing either all up or all down. In bosonic language, these latter configurations correspond to the completely full/empty insulating configurations.

At this point we can calculate the following quantities. First, the density of particles is:

$$\begin{aligned} \rho_{\text{MF}} &= \frac{1}{N} \sum_i {}_{\text{MF}}\langle 0 | \hat{a}_i^\dagger \hat{a}_i | 0 \rangle_{\text{MF}} = \frac{1}{2} + \frac{1}{2N} \sum_i \cos \theta_i \\ &= \frac{1}{2} + \frac{1}{4} (\cos \theta_1 + \cos \theta_2). \end{aligned} \quad (10)$$

Next, the free energy becomes

$$\begin{aligned} \Omega_{\text{MF}} &= {}_{\text{MF}}\langle 0 | \hat{H} | 0 \rangle_{\text{MF}} = -\frac{dt}{2} \sin \theta_1 \sin \theta_2 - \frac{\mu}{2} \\ &\quad - \frac{1}{4} (\mu + A) \cos \theta_1 - \frac{1}{4} (\mu - A) \cos \theta_2, \end{aligned} \quad (11)$$

and the fraction of bosons in the zero-momentum mode ρ_0 is calculated as:

$$\begin{aligned} \rho_{0,\text{MF}} &= \frac{1}{N} {}_{\text{MF}}\langle 0 | \hat{a}_{k=0}^\dagger \hat{a}_{k=0} | 0 \rangle_{\text{MF}} \\ &= \frac{1}{4N^2} \sum_{i,j} \sin \theta_i \sin \theta_j = \frac{1}{16} (\sin \theta_1 + \sin \theta_2)^2. \end{aligned} \quad (12)$$

The superfluid density ρ_s requires a special treatment of the boundary conditions. As is well known,²³ one can relate the superfluid density to the “spin stiffness”. To accomplish this, one needs to compare Ω (the free energy) of the system under periodic conditions with the free energy under a “twist” in the boundary conditions along one of the linear directions (say, the x direction). In the periodic case, which we treated above, the azimuthal angles φ_j were all identical. To implement a twist, we take this angle to be site-dependent and with a constant gradient such that the total twist across the system in

the x direction is π , namely $\delta\varphi = \varphi_{j+\hat{x}} - \varphi_j = \pi/L$. Within the mean-field treatment, one can show that addition of this gradient is equivalent to substituting $t \rightarrow t/d[(d-1) + \cos \delta\varphi]$. Now, the square of the gradient twist is related to the superfluid density via,^{15,23}

$$\Omega_{\text{twisted}} - \Omega = t\rho_s \delta\varphi^2, \quad (13)$$

which in turn yields the simple expression

$$\rho_s = -\frac{1}{2d} \frac{\partial \Omega}{\partial t}. \quad (14)$$

Setting $\mu = 0$, this expression for the superfluid density coincides with that of $\rho_{0,\text{MF}}$:

$$\rho_{s,\text{MF}} = \rho_{0,\text{MF}} = \begin{cases} \frac{1}{4} - \left(\frac{A}{4dt}\right)^2, & \frac{A}{2dt} < 1 \\ 0, & \frac{A}{2dt} \geq 1 \end{cases}, \quad (15)$$

giving the critical value for the phase transition $A_c/(2dt) = 1$. Figures 8 and 9 show: (a) the free energy, (b) the superfluid density, (c) the fraction of bosons in the zero-momentum mode, and (d) the compressibility of the system as a function of $A/(2dt)$ in two and three dimensions. The dashed and solid curves represent the mean-field and exact results, respectively. As one can immediately see, the critical values obtained within the mean-field approximation do not agree with the exact-numerical results. In two dimensions the error is $\approx 100\%$ and in three dimensions, it is $\approx 50\%$.

B. Adding spin-wave corrections

As pointed out earlier, the addition of spin-wave corrections yields virtually exact results in the homogeneous case in two dimensions.¹⁵ For the reader's convenience, we review the mean-field calculations of the homogeneous ($A = 0$) case and its spin-wave corrections in Appendix A (thereby also correcting some misprints that appeared in the original manuscript examining this case, Ref. 15). Let us see how the mean-field results are modified by the addition of spin-wave corrections in our case. To include these, we proceed in the usual way.^{24,25,26,27} We first introduce a set of local rotations that align the \hat{z} direction of each of the spins with its mean field orientation. This is accomplished by switching to new spin operators defined by

$$\begin{pmatrix} S_j'^x \\ S_j'^y \\ S_j'^z \end{pmatrix} = R(\theta_j, \varphi_j) \begin{pmatrix} S_j^x \\ S_j^y \\ S_j^z \end{pmatrix} \quad (16)$$

where $R(\theta_j, \varphi_j)$ is a 3×3 rotation matrix. The corresponding new annihilation and creation operators $\hat{b}_j \leftrightarrow S_j'^-$ and $\hat{b}_j^\dagger \leftrightarrow S_j'^+$ describe low-energy fluctuations about the mean-field ground state – these are spin waves. They

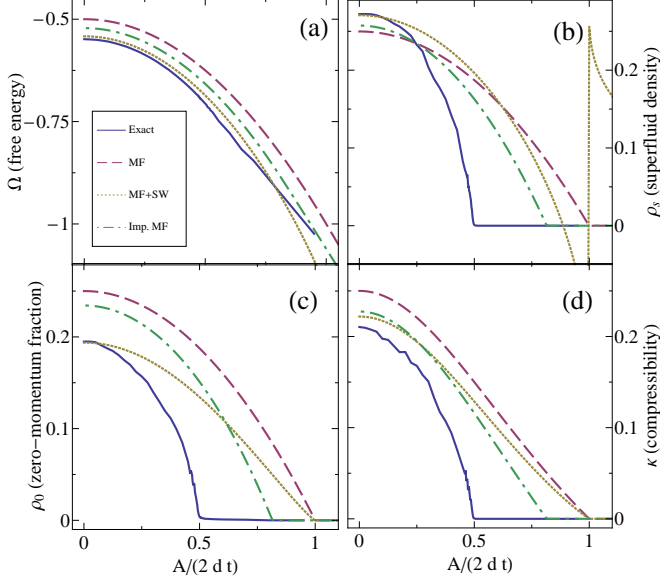


FIG. 8: (Color online) Thermodynamic quantities in two dimensions. (a) Free energy, (b) superfluid density, (c) the fraction of bosons in the zero-momentum mode, and (d) compressibility as a function of $A/(2dt)$. The solid lines indicate the exact SSE results (64×64 sites, $\beta = 96$), whereas the dashed, dotted and dash-dotted lines indicate the mean-field, mean-field plus spin-waves and improved mean-field results, respectively.

too obey hardcore bosons commutation relations. Substituting these expressions into our Hamiltonian, and ignoring cubic and quartic terms in these bosonic operators (thus assuming a dilute gas of spin waves), the new Hamiltonian reads

$$\begin{aligned} \hat{H}_{\text{SW}} = & \hat{H}_{\text{MF}} + D \sum_i \hat{b}_i^\dagger \hat{b}_i + C \sum_i (-1)^{\sigma(i)} \hat{b}_i^\dagger \hat{b}_i \\ & + B \sum_{\langle ij \rangle} (\hat{b}_i^\dagger \hat{b}_j^\dagger + \hat{b}_i \hat{b}_j) - \frac{A}{2} \sum_{\langle ij \rangle} (\hat{b}_i^\dagger \hat{b}_j + \hat{b}_i \hat{b}_j^\dagger), \end{aligned} \quad (17)$$

where the coefficients are

$$A = t(1 + \cos \theta_1 \cos \theta_2), \quad (18a)$$

$$B = t/2(1 - \cos \theta_1 \cos \theta_2), \quad (18b)$$

$$C = dt(\mu_1 \cos \theta_1 - \mu_2 \cos \theta_2), \quad (18c)$$

$$D = dt(2 \sin \theta_1 \sin \theta_2 + \mu_1 \cos \theta_1 + \mu_2 \cos \theta_2). \quad (18d)$$

This quadratic Hamiltonian can be diagonalized by first going to Fourier space, using $\hat{b}_j = N^{-1/2} \sum_k e^{2\pi i k j / L} \hat{b}_k$. This in turn yields the Hamiltonian:

$$\begin{aligned} \hat{H}_{\text{SW}} = & \hat{H}_{\text{MF}} + \sum_k (D - A\gamma_k) \hat{b}_k^\dagger \hat{b}_k + C \sum_k \hat{b}_k^\dagger \hat{b}_{k+L/2} \\ & + B \sum_k \gamma_k (\hat{b}_k^\dagger \hat{b}_{L-k}^\dagger + \hat{b}_k \hat{b}_{L-k}), \end{aligned} \quad (19)$$

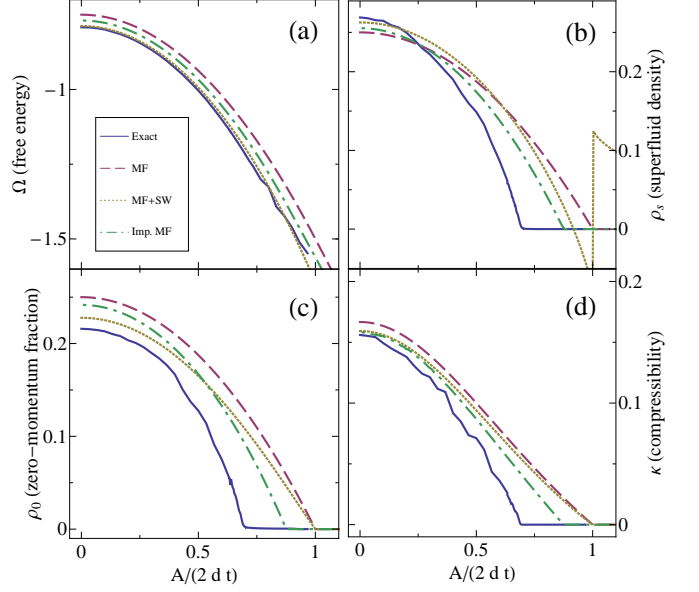


FIG. 9: (Color online) Thermodynamic quantities in three dimensions. (a) Free energy, (b) superfluid density, (c) the fraction of bosons in the zero-momentum mode, and (d) compressibility as a function of $A/(2dt)$. The solid lines indicate the exact SSE results ($16 \times 16 \times 16$ sites, $\beta = 40$), whereas the dashed, dotted and dash-dotted lines indicate the mean-field, mean-field plus spin-waves and improved mean-field results, respectively.

where, $\gamma_k = \sum_{i=1}^d \cos(\frac{2\pi k_i}{L})$, and $k_1 \dots k_d$ are the components of the momentum vector in each of the directions. We note that the Fourier-space operators \hat{b}_k and \hat{b}_k^\dagger no longer obey the hardcore bosons commutation relations. However, as these field operators are only excitations about the ground state, we find it sufficient to treat them as soft-core bosons. At this point, our Hamiltonian may be diagonalized in a straightforward manner (we review the diagonalization process in Appendix B). Once diagonalized, the Hamiltonian takes the form

$$\hat{H}_{\text{SW}} = \hat{H}_{\text{MF}} + \sum_k \Lambda_k \hat{\eta}_k^\dagger \hat{\eta}_k + E_0, \quad (20)$$

where the Λ_k 's are energy levels and E_0 is the correction to the ground-state energy of the system, given by:

$$E_0 = \frac{1}{4} \sum_k \left(-2D + \sqrt{(A^2 - 4B^2)\gamma_k^2 + D^2 + C^2 + 2\sqrt{(DC)^2 + [(AD)^2 - (2BC)^2]\gamma_k^2}} \right. \\ \left. + \sqrt{(A^2 - 4B^2)\gamma_k^2 + D^2 + C^2 - 2\sqrt{(DC)^2 + [(AD)^2 - (2BC)^2]\gamma_k^2}} \right). \quad (21)$$

The operators $\hat{\eta}_k^\dagger$ and $\hat{\eta}_k$ in Eq. (20) are modified spin-wave creation and annihilation operators, respectively, and are each a linear combination of $\hat{b}_k, \hat{b}_{L-k}, \hat{b}_{k+L/2}, \hat{b}_{L/2-k}$ and their adjoints. The coefficients of these linear combinations are fixed during the diagonalization process, and using them, all physical observables can be calculated in a straightforward manner (we elaborate on this matter in Appendix B).

The results of the spin-wave analysis are indicated by the dotted lines in Figs. 8 (two-dimensions) and 9 (three dimensions). They show: (a) the free energy, (b) the superfluid density, (c) the fraction of bosons in the zero-momentum mode, and (d) the compressibility, after the addition of spin-wave corrections, as a function of $A/(2dt)$.

As one can see in those figures, in the superfluid phase, the spin-wave corrected values for the free energy are almost on top of the exact-numerical ones; and more so in the three-dimensional case than in the two-dimensional one. As for the other measured observables, the spin-wave corrections are clearly an improvement over the mean-field results. Unfortunately however, as one approaches the phase transition itself, the spin-wave corrections lose their accuracy, eventually leaving the phase-transition at its mean-field value, namely at $A_c/(2dt) = 1$.

Another issue worth noting here is the behavior of the spin-wave corrected superfluid density [Figs. 8(b) and 9(b)] in the vicinity of the predicted phase transition, $A/(2dt) = 1$. On the superfluid side of the transition the superfluid density becomes negative, indicating the breakdown of the spin-wave approximation for that quantity. The transition point is still signaled by a discontinuity in ρ_s . However, the overall behavior of the superfluid density around the transition point is clearly an artifact of the spin-wave approximation and should not be considered further.

C. Improved mean-field approach

Having seen that spin-wave corrections, albeit accurate in the weak-potential regime, do not modify the critical point predicted by the mean-field solution, we have devised an improved mean-field approach. As we show now, this method provides a significant improvement over the mean-field results (and the spin-wave corrections) discussed previously, particularly in the context of the loca-

tion of the critical point.

We start with a variational ansatz which, as before, is a product state. However, this time we do not choose a product of single-site wave-functions. The new ansatz is a product of wave-functions each describing the state of a ‘block’ of 2^d sites, such that with this block as the basic cell, the model turns homogeneous. In two dimensions a block consists of 2×2 cells (as shown in Fig. 10) each of which is described by the general wave function

$$|0\rangle_{\text{IMF}} = \prod_{\text{blocks}}^{\otimes} \left(\sum_{i,j,k,l \in \{\downarrow, \uparrow\}} c_{ijkl} |ijkl\rangle \right), \quad (22)$$

where the generalization to three dimensions, in which case the basic block is a $2 \times 2 \times 2$ cell, is straightforward (note that the coefficients for each of the blocks are the same). As before, we minimize the free energy $\Omega_{\text{IMF}} = \text{IMF} \langle 0 | \hat{H} | 0 \rangle_{\text{IMF}}$ with respect to the coefficients c_{ijkl} of the wave function (this time we do so numerically). The results of this approximation are given by the dash-dotted lines in Figs. 8 and 9. They depict: (a) the free energy, (b) the superfluid density, (c) the fraction of bosons in the zero-momentum mode, and (d) the compressibility, as a function of $A/(2dt)$.

As the figures indicate, in most instances, the results of this method are more accurate than those of the previous approximation schemes, in particular, for the location of the phase transition. The critical values given by this approximation are $A_c/(2dt) = 0.815$ in two dimensions ($\approx 60\%$ error) and $A_c/(2dt) = 0.875$ in three dimensions ($\approx 24\%$ error). Also, we note that while the spin-wave corrected values for the various thermodynamic quantities are a better approximation in the weak potential (small $A/(2dt)$) regime, as one moves away from this region, the improved mean-field technique proves to be a better estimator for all quantities but the free energy.

V. CONCLUSIONS

We have studied the superfluid to Mott-insulator phase transition of hardcore bosons in a period-two superlattice in two and three dimensions. We focused on the case where the system is at half filling, for which the quantum phase transition belongs to the $(d+1)$ dimensional XY universality class. Using quantum Monte Carlo simulations and finite size scaling, we have accurately determined the critical value of the alternating

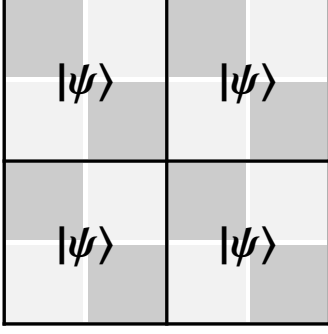


FIG. 10: In the ‘improved mean-field’ case, a larger unit-cell is defined. In the two-dimensional case at hand, the new cell consists of 2×2 sites. With this new definition the model turns homogeneous and a product of identical wave functions is then guessed as a solution.

potential parameter A at which the phase transition occurs. In two dimensions, our result agrees with a previous calculation.²¹

We have devised a mean-field approximation scheme which is based on the underlying homogeneity of the problem. This approach provides an analytical description of the superfluid-to-Mott-insulator transition and gives an estimate of the critical value for the transition with (around) one half the error of the usual Gutzwiller ansatz, i.e., it is a big improvement in terms of the location of the critical point.

The spin-wave corrections turned out to be a very useful method, especially in the superfluid phase, where the spin-wave corrected estimation of the free-energy is very close to the exact values. However, as one moves away from the weak potential regime, the spin-wave corrections become more and more inaccurate, and their predictions of the critical points eventually coincide with those of the mean-field approach.

Acknowledgments

This work was supported by startup funds from Georgetown University and by the US Office of Naval Research. We thank Tommaso Roscilde and Valery G. Rousseau for useful discussions.

APPENDIX A: MEAN-FIELD RESULTS AND SPIN-WAVE CORRECTIONS IN THE HOMOGENEOUS CASE

In what follows, we briefly review the results of the mean-field approximation of Sec. IV A and its spin-wave corrections in the homogeneous ($A = 0$) case for arbitrary values of μ .

Starting with the ansatz given in Eq. (7), minimization of the free energy Eq. (8) with respect to the spin

orientation angles yields

$$\cos \theta_j = \frac{\mu}{2dt}, \quad (\text{A1})$$

where the azimuthal angle takes on, once again, a constant yet arbitrary value $\varphi_j = \Phi$. The density of particles becomes

$$\begin{aligned} \rho_{\text{MF}} &= \frac{1}{N} \sum_i \text{MF} \langle 0 | \hat{a}_i^\dagger \hat{a}_i | 0 \rangle_{\text{MF}} = \frac{1}{2} + \frac{1}{2N} \sum_i \cos \theta_i \\ &= \frac{1}{2} \left(1 + \frac{\mu}{2dt} \right), \end{aligned} \quad (\text{A2})$$

and the free energy is

$$\begin{aligned} \Omega_{\text{MF}} &= \text{MF} \langle 0 | \hat{H} | 0 \rangle_{\text{MF}} = -\frac{dt}{2} \sin^2 \theta - \frac{1}{2} \mu (1 + \cos \theta) \\ &= -\frac{1}{2} dt \left(1 + \frac{\mu}{2dt} \right)^2. \end{aligned} \quad (\text{A3})$$

The fraction of bosons in the zero-momentum mode turns out to be

$$\begin{aligned} \rho_{0,\text{MF}} &= \frac{1}{N} \text{MF} \langle 0 | \hat{a}_{k=0}^\dagger \hat{a}_{k=0} | 0 \rangle_{\text{MF}} \\ &= \frac{1}{4N^2} \sum_{i,j} \sin \theta_i \sin \theta_j = \frac{1}{4} \left[1 - \left(\frac{\mu}{2dt} \right)^2 \right]. \end{aligned} \quad (\text{A4})$$

Using Eq. (14), it can be easily shown that the expression for the superfluid density $\rho_{s,\text{MF}}$ in the homogeneous case coincides with the expression obtained for $\rho_{0,\text{MF}}$ above (as is the case with the alternating potential).

The addition of spin-wave corrections to the mean-field results is carried out in exactly the same manner as with the staggered potential. The Hamiltonian in this case has the same form as the one given in Eq. (17) but with coefficients

$$A = t \left[1 + \left(\frac{\mu}{2dt} \right)^2 \right], \quad (\text{A5a})$$

$$B = \frac{t}{2} \left[1 - \left(\frac{\mu}{2dt} \right)^2 \right], \quad (\text{A5b})$$

$$C = 0, \quad (\text{A5c})$$

$$D = 2dt. \quad (\text{A5d})$$

The spin-wave field operators which diagonalize the Hamiltonian are given by the simple relation:¹⁵

$$\hat{b}_k = \cosh \phi_k \hat{\eta}_k - \sinh \phi_k \hat{\eta}_{L-k}^\dagger, \quad (\text{A6})$$

with ϕ_k obeying

$$\sinh^2 \phi_k = \frac{1}{2} \left(\frac{D - A\gamma_k}{\sqrt{(D - A\gamma_k)^2 - (2B\gamma_k)^2}} - 1 \right), \quad (\text{A7a})$$

$$\cosh^2 \phi_k = \frac{1}{2} \left(\frac{D - A\gamma_k}{\sqrt{(D - A\gamma_k)^2 - (2B\gamma_k)^2}} + 1 \right), \quad (\text{A7b})$$

and so, the various spin-wave corrected quantities may be written explicitly: The corrected density of particles is

$$\rho_{\text{SW}} = \rho_{\text{MF}} - \frac{1}{N} \frac{\mu}{2dt} \sum_{k \neq 0} \sinh^2 \phi_k, \quad (\text{A8})$$

and the free energy becomes

$$\Omega_{\text{SW}} = \Omega_{\text{MF}} + \frac{1}{2} \sum_{k \neq 0} \left[\sqrt{(D - A\gamma_k)^2 - (2B\gamma_k)^2} - (D - A\gamma_k) \right]. \quad (\text{A9})$$

Using Eq. (14), the superfluid density immediately follows. Finally, the fraction of bosons in the zero-momentum mode turns out to be:

$$\rho_{0,\text{SW}} = \rho_{0,\text{MF}} - \frac{1}{N} \left[1 - \left(\frac{\mu}{2dt} \right)^2 \right] \sum_{k \neq 0} \sinh^2 \phi_k. \quad (\text{A10})$$

APPENDIX B: DIAGONALIZATION OF QUADRATIC BOSONIC HAMILTONIANS

Following the prescription given in Ref. 28 for the diagonalization of fermionic quadratic Hamiltonians, we provide here the analogous prescription for the diagonalization of bosonic quadratic Hamiltonians of the general form

$$\hat{H} = \sum_{k,m} \left(A_{km} \hat{b}_k^\dagger \hat{b}_m + \frac{1}{2} B_{km} (\hat{b}_k^\dagger \hat{b}_m^\dagger + \hat{b}_k \hat{b}_m) \right), \quad (\text{B1})$$

where \hat{b}_k and \hat{b}_k^\dagger are bosonic annihilation and creation operators, respectively, and A_{km} and B_{km} are real-valued and symmetric. For the spin-wave Hamiltonian of Eq. (19), the coefficients are

$$A_{km} = (D - A\gamma_k) \delta_{km} + C \delta_{k,m+L/2}, \quad (\text{B2a})$$

$$B_{km} = 2B\gamma_k \delta_{k,L-m}. \quad (\text{B2b})$$

The diagonalization process starts by defining the following linear transformation

$$\hat{\eta}_k = \sum_m \left(g_{km} \hat{b}_m + h_{km} \hat{b}_m^\dagger \right), \quad (\text{B3})$$

where g_{km} and h_{km} are real-valued and we require $\hat{\eta}_k$ and $\hat{\eta}_k^\dagger$ be bosonic operators. This is enforced by the constraint

$$\delta_{km} = [\eta_k, \eta_m^\dagger] = \sum_l (g_{kl} g_{ml} - h_{kl} h_{ml}). \quad (\text{B4})$$

The coefficients g_{km} and h_{km} are determined in such a way that the transformed Hamiltonian takes the diagonal form

$$H = \sum_k \Lambda_k \hat{\eta}_k^\dagger \hat{\eta}_k + E_0, \quad (\text{B5})$$

once the $\hat{\eta}_k$'s are substituted for the \hat{b}_k 's, and $E_0 = -\sum_{k,m} \Lambda_m h_{mk}^2$. As the new Hamiltonian is already in diagonal form, the new field operators obey the eigenvalue equation

$$[\hat{\eta}_k, \hat{H}] = \Lambda_k \hat{\eta}_k. \quad (\text{B6})$$

Plugging in the transformations given in Eqs. (B3), we obtain the relations

$$\Lambda_k g_{km} = \sum_l (g_{kl} A_{lm} - h_{kl} B_{ml}), \quad (\text{B7a})$$

$$\Lambda_k h_{km} = \sum_l (g_{kl} B_{ml} - h_{kl} A_{lm}). \quad (\text{B7b})$$

These relations may be further simplified by defining the new coefficients

$$\phi_{km} = g_{km} + h_{km}, \quad (\text{B8a})$$

$$\psi_{km} = g_{km} - h_{km}, \quad (\text{B8b})$$

for which, the constraint (B4) translates to

$$\frac{1}{2} \sum_l (\phi_{kl} \psi_{ml} + \psi_{kl} \phi_{ml}) = \delta_{km}. \quad (\text{B9})$$

With the above definitions, Eqs. (B7) may be cast in vector notation:

$$\phi_k (\mathbf{A} - \mathbf{B}) = \Lambda_k \psi_k, \quad (\text{B10a})$$

$$\psi_k (\mathbf{A} + \mathbf{B}) = \Lambda_k \phi_k. \quad (\text{B10b})$$

These can be solved by simply plugging each of these equations into the other, resulting in the eigenvalue equations

$$\psi_k (\mathbf{A} + \mathbf{B})(\mathbf{A} - \mathbf{B}) = \Lambda_k^2 \psi_k, \quad (\text{B11a})$$

$$\phi_k (\mathbf{A} - \mathbf{B})(\mathbf{A} + \mathbf{B}) = \Lambda_k^2 \phi_k. \quad (\text{B11b})$$

These equations are to be solved by standard techniques. Once the Λ_k 's, ϕ_k 's and ψ_k 's are found, all physical observables can be readily calculated: First, the observable of interest should be expressed in terms of normal-ordered $\hat{\eta}_k$'s. This may be accomplished by using the inverse of the transformation given in Eq. (B3):

$$\hat{b}_k = \frac{1}{2} \sum_m \left((\phi_{km}^{-1} + \psi_{km}^{-1}) \hat{\eta}_m + (\phi_{km}^{-1} - \psi_{km}^{-1}) \hat{\eta}_m^\dagger \right). \quad (\text{B12})$$

As a next step, one should use the fact that as excitations, the $\hat{\eta}_k$'s obey $\hat{\eta}_k |0\rangle_{\text{MF}} = 0$. This leads to

$$\langle 0 | \hat{b}_k^\dagger \hat{b}_m | 0 \rangle_{\text{MF}} = \frac{1}{4} \sum_l (\phi_{kl}^{-1} - \psi_{kl}^{-1}) (\phi_{ml}^{-1} - \psi_{ml}^{-1}). \quad (\text{B13})$$

As an example, consider the spin-wave corrected density of particles in our model. It is calculated as

$$\begin{aligned}
\rho_{\text{SW}} &= \frac{1}{N} \sum_i \text{MF} \langle 0 | \hat{a}_i^\dagger \hat{a}_i | 0 \rangle_{\text{MF}} = \rho_{\text{MF}} - \frac{1}{N} \sum_i \text{MF} \langle 0 | \hat{b}_i^\dagger \hat{b}_i \cos \theta_i | 0 \rangle_{\text{MF}} \\
&= \rho_{\text{MF}} - \frac{1}{2N} (\cos \theta_1 + \cos \theta_2) \sum_k \text{MF} \langle 0 | \hat{b}_k^\dagger \hat{b}_k | 0 \rangle_{\text{MF}} - \frac{1}{2N} (\cos \theta_1 - \cos \theta_2) \sum_k \text{MF} \langle 0 | \hat{b}_k^\dagger \hat{b}_{k+L/2} | 0 \rangle_{\text{MF}} \\
&= \rho_{\text{MF}} - \frac{1}{8N} \left((\cos \theta_1 + \cos \theta_2) \sum_{mk} (\phi_{km}^{-1} - \psi_{km}^{-1})^2 + (\cos \theta_1 - \cos \theta_2) \sum_{mk} (\phi_{km}^{-1} - \psi_{km}^{-1}) (\phi_{(k+L/2),m}^{-1} - \psi_{(k+L/2),m}^{-1}) \right).
\end{aligned} \tag{B14}$$

All other observables may be calculated in the same manner.

* Electronic address: itayhe@physics.georgetown.edu

† Electronic address: mrigol@physics.georgetown.edu

¹ M. Greiner, O. Mandel, T. Esslinger, T. E. Hänsch, and I. Bloch, *Nature (London)* **415**, 39 (2002).

² M. Greiner, O. Mandel, T. E. Hänsch, and I. Bloch, *Nature (London)* **419**, 51 (2002).

³ S. Sachdev, *Quantum Phase Transitions* (Cambridge University Press, Cambridge, England, 1999).

⁴ M. P. A. Fisher, P. B. Weichman, G. Grinstein, and D. S. Fisher, *Phys. Rev. B* **40**, 546 (1989).

⁵ D. Jaksch, C. Bruder, J. I. Cirac, C. W. Gardiner, and P. Zoller, *Phys. Rev. Lett.* **81**, 3108 (1998).

⁶ W. Zwerger, *J. Opt. B: Quantum Semiclassical*, **Opt.** **5**, 9 (2003).

⁷ I. Bloch, J. Dalibard, and W. Zwerger, *Rev. Mod. Phys.* **80**, 885 (2008).

⁸ E. H. Lieb and F. Y. Wu, *Physica A* **321**, 1 (2003).

⁹ M. Aizenman, E. H. Lieb, R. Seiringer, J. P. Solovej, and J. Yngvason, *Phys. Rev. A* **70**, 023612 (2004).

¹⁰ V. G. Rousseau, D. P. Arovas, M. Rigol, F. Hébert, G. G. Batrouni, and R. T. Scalettar, *Phys. Rev. B* **73**, 174516 (2006).

¹¹ M. Rigol and A. Muramatsu, *Phys. Rev. A* **70**, 031603(R) (2004); *Phys. Rev. A* **72**, 013604 (2005).

¹² M. Rigol, A. Muramatsu, and M. Olshanii, *Phys. Rev. A* **74**, 053616 (2006).

¹³ A. W. Sandvik, *Phys. Rev. B* **59**, R14157 (1999).

¹⁴ A. Dorneich and M. Troyer, *Phys. Rev. E* **64**, 066701 (2001).

¹⁵ K. Bernardet, G. G. Batrouni, J.-L. Meunier, G. Schmid, M. Troyer and A. Dorneich, *Phys. Rev. B* **65**, 104519 (2002).

¹⁶ C. Bruder, R. Fazio and G. Schön, *Annalen der Physik* **14**, 566 (2005).

¹⁷ S. Peil, J. V. Porto, B. Laburthe Tolra, J. M. Obrecht, B. E. King, M. Subottin, S. L. Rolston, and W. D. Phillips, *Phys. Rev. A* **67**, 051603(R) (2003).

¹⁸ J. Sebby-Strabley, M. Anderlini, P. S. Jessen, and J. V. Porto, *Phys. Rev. A* **73**, 033605 (2006).

¹⁹ J. Sebby-Strabley, B. L. Brown, M. Anderlini, P. J. Lee, W. D. Phillips, J. V. Porto, and P. R. Johnson, *Phys. Rev. Lett.* **98**, 200405 (2007).

²⁰ P. J. Lee, M. Anderlini, B. L. Brown, J. Sebby-Strabley, W. D. Phillips, and J. V. Porto, *Phys. Rev. Lett.* **99**, 020402 (2007).

²¹ A. Priyadarshree, S. Chandrasekharan, J.-W. Lee, and H. U. Baranger, *Phys. Rev. Lett.* **97**, 115703 (2006).

²² T. Matsubara and H. Matsuda, *Prog. Theor. Phys.* **16**, 569 (1956).

²³ M. E. Fisher, M. N. Barber, and D. Jasnow, *Phys. Rev. A* **8**, 1111 (1973).

²⁴ K. S. Liu and M. E. Fisher, *J. Low Temp. Phys.* **10**, 655 (1973).

²⁵ Yi-Chen Cheng, *Phys. Rev. B* **23**, 157 (1981).

²⁶ R. T. Scalettar, G. G. Batrouni, A. P. Kampf, and G. T. Zimanyi, *Phys. Rev. B* **51**, 8467 (1995).

²⁷ G. Murthy, D. Arovas, and A. Auerbach, *Phys. Rev. B* **55**, 3104 (1997).

²⁸ E. Lieb, T. Schultz and D. Mattis, *Annals of Physics* **16**, 407 (1961).

²⁹ For homogeneous systems, the number of bosons in the zero-momentum mode coincides with the condensate occupation. However, this need not be the case in general, as the condensate occupation is defined as the largest eigenvalue of the one-particle density matrix. The latter quantity will in general be different from the occupation of the zero-momentum state if the system is inhomogeneous.¹²